PHYSICAL REVIEW D **74,** 063506 (2006)

Alignment tests for low CMB multipoles

L. Raul Abramo*
Instituto de Física, Universidade de São Paulo CP 66318, CEP 05315-970 São Paulo, Brazil

Armando Bernui,† Ivan S. Ferreira,‡ Thyrso Villela,§ and Carlos Alexandre Wuensche‖
Divisão de Astrofísica, Instituto Nacional de Pesquisas Espaciais Av. dos Astronautas, 1.758, CEP 12227-010, São José dos Campos, Brazil

(Received 10 May 2006; published 7 September 2006)

We investigate the large scale anomalies in the angular distribution of the cosmic microwave background radiation as measured by WMAP using several tests. These tests, based on the multipole vector expansion, measure correlations between the phases of the multipoles as expressed by the directions of the multipole vectors and their associated normal planes. We have computed the probability distribution functions for 46 such tests, for the multipoles $\ell = 2 - 5$. We confirm earlier findings that point to a high level of alignment between $\ell = 2$ (quadrupole) and $\ell = 3$ (octopole), but with our tests we do not find significant planarity in the octopole. In addition, we have found other possible anomalies in the alignment between the octopole and the $\ell = 4$ (hexadecupole) components, as well as in the planarity of $\ell = 4$ and $\ell = 5$. We introduce the notion of a global anomaly statistic to estimate the relevance of the low-multipoles tests of non-Gaussianity. We show that, as a result of these tests, the CMB maps which are most widely used for cosmological analysis lie within the $\sim$10% of randomly generated maps with lowest global anomaly statistics.

DOI: 10.1103/PhysRevD.74.063506 PACS numbers: 98.80.Es, 98.65.Dx, 98.70.Vc

I. INTRODUCTION

The cosmic microwave background (CMB) anisotropies have been measured with exquisite accuracy by the Wilkinson Microwave Anisotropies Probe (WMAP), and the impact on cosmology has been profound [1–4]. However, as the ΛCDM cosmological model becomes standard lore and the parameter space becomes narrower, the focus naturally drifts to the apparent anomalies. Among sources of concern that have survived the WMAP 3-year data are the lack of large-angle correlations [1,2,4], which is mainly due to the low value of the cosmic quadrupole [4–8], and the alignment between the quadrupole ($\ell = 2$) and octopole ($\ell = 3$) [4,5,9–15].

The combined statistics of the low quadrupole and of the quadrupole-octopole alignment, which were already in the COBE data [16,17], can only be matched by 0.01% of Gaussian random maps—see, for instance, [5]. However, caution should be taken in the interpretation of that result as an outright indication of violations of statistical isotropy, since this tiny probability was in fact constructed *a posteriori*, by multiplying the probabilities of two statistical tests which were previously thought to be unrelated.

Several recent works have reported anomalies in the data: the low-order multipole values [1,2,4,6,15,18–20]; the alignment of some low-order multipoles [5,15,21–23]; an unexpected asymmetric distribution on the sky of the large-scale power of CMB data [14,24–27]; indications for a preferred direction of maximum asymmetry [9,25,27–30]; as well as apparent non-Gaussian features detected via the wavelet method or other analyses [31–36]. These anomalies have motivated many explanations, such as compact topologies [37,38], a broken or suppressed spectrum at large scales [39–44], oscillations superimposed on the primordial spectrum of density fluctuations [45–47], anisotropic cosmological models [48–50] and possible extended foregrounds that could be affecting the CMB [10,51–54].

In this article we examine the multipoles $\ell = 2 - 5$ and search for anomalies in their phase correlations. We measure these correlations through alignments between the multipole vectors or through their associated normal planes [9]. We also look for evidence of planarity (or *self-alignments*) in each individual multipole, and for evidence of alignments between the multipole and normal vectors with some specific directions in the sky, such as the dipole axis, the ecliptic axis and the Galactic poles axis. In total we have considered 38 tests of alignments between multipoles, plus 8 tests of alignments of the multipoles with *a priori* directions. We have computed the probability distribution functions (PDFs) for those tests using 300 000 mock maps.

For the statistical analyses performed here, we need the $a_{\ell m}$'s ($\ell = 2 - 5$) of each CMB map under investigation. The corresponding $a_{\ell m}$'s were extracted, after applying the Kp2 WMAP mask (to minimize foreground contaminations from the beginning), through the HEALPix routines [55]. Our statistical tools were then used to analyze the WMAP 1-year and 3-year data Internal Linear Com-

*Electronic address: abramo@fma.if.usp.br
†Electronic address: bernui@das.inpe.br
‡Electronic address: ivan@das.inpe.br
§Electronic address: thyrso@das.inpe.br
‖Electronic address: alex@das.inpe.br

bination maps [1,4] (henceforth ILC), the co-added 1-year and 3-year WMAP data, as well as the *cleaned* CMB maps of Tegmark *et al.* [13,15] based on 1-year WMAP data (henceforth TOH).

This paper is organized as follows. In Sec. II we summarize the multipole vector formalism and the several different statistics that can be used to test for alignments and phase correlations within a given multipole. In Sec. III we briefly describe the CMB maps used. Section IV presents our statistical tests and the results of the PDF computations for those tests. We also analyze the salient features of the CMB maps and discuss which tests can be considered anomalous, and of those, which are robust and which are most sensitive to noise. The conclusions are presented in Sec. V.

II. MULTIPOLE VECTORS, NORMAL VECTORS AND STATISTICS OF PHASE CORRELATIONS

Multipole vectors were introduced in CMB data analysis by Copi *et al.* [9], and Katz and Weeks [11,12] found an elegant algebraic method to compute the multipole vectors given the spherical harmonic components $a_{\ell m}$—see also [56] for an alternative algebraic method and [5,10,14] for purely numerical methods. The multipole vectors are essentially eigenvectors—i.e., they are solutions of a set of polynomial equations whose parameters are the multipole components $a_{\ell m}$.

The idea of the multipole vector representation goes back to J. C. Maxwell in the XIXth century: the multipole decomposition of a field $f(\theta, \phi)$ on S^2 implies that for each multipole ℓ there are ℓ eigenvectors of norm unity, $\hat{n}^{(\ell,p)}$. Since there are only 2ℓ phases for each multipole, the spherical harmonic representation and the multipole vector representation have the same number of degrees of freedom in each individual multipole:

$$\frac{\Delta T_\ell(\theta,\varphi)}{T} = \sum_{m=-\ell}^{\ell} a_{\ell m} Y_{\ell m}(\theta,\varphi) = D_\ell \prod_{p=1}^{\ell} \hat{n}^{(\ell,p)} \cdot \hat{n}(\theta,\phi) - Z_{\ell-1}(\theta,\varphi), \quad (1)$$

where $Z_{\ell-1}$ just subtracts the residual $\ell' < \ell$ total angular momentum parts of the product expansion, and is irrelevant to our analysis—see [11] for an enhanced discussion of the multipole vector expansion.

It can be seen from the product expansion above that, whenever using the multipole vectors to test for alignments, it is irrelevant what the amplitudes of the multipoles are—just their phases matter. This is the main feature of the tests based on the multipole vectors that sets them apart from other tests of non-Gaussianity.

Notice that, contrary to the C_ℓ's, which are always positive-definite, the D_ℓ's of Eq. (1) can be either negative or positive. Because of the product expansion in the right-hand-side of Eq. (1), switching the sign of D_ℓ is equivalent to switching the signs of an odd number of multipole vectors, and switching the signs of an even number of multipole vectors leaves the sign of D_ℓ invariant. Therefore, the product expansion in Eq. (1) has a sign degeneracy in the amplitudes D_ℓ as well as in the multipole vectors $\hat{n}^{(\ell,p)}$.

This "reflection symmetry" $\hat{n}^{(\ell,p)} \leftrightarrow -\hat{n}^{(\ell,p)}$ implies that the multipole vectors define only directions [11], hence they are "vectors without arrowheads" living on the half-sphere with antipodal points identified, or $S^2/\mathbb{Z}_2$. This space is also known in the literature as the real projective space $\mathbb{R}P^2$, and is useful in the characterization of nematic liquid crystals, where the orientation of the molecules is an order parameter—but it makes no difference where heads and tails are [57].

It is extremely useful to represent these directions as vectors, but for that we will need to cope with the degeneracy in representing these directions. For each multipole order ℓ there is a $2^{\ell-1}$-fold degeneracy in the signs (or orientations) of the multipole vectors—corresponding to the ℓ signs of the multipole vectors that can be switched arbitrarily, divided by two to account for an irrelevant overall sign which is determined by D_ℓ. We can break this degeneracy by always working in one particular hemisphere, and any such choice will automatically determine the signs (orientations) of all multipole vectors—as well as the sign of the D_ℓ's. However, we should be aware that in doing so we are necessarily picking *one* of the $2^{\ell-1}$ possible sign conventions in the product expansion of Eq. (1). As we will discuss below, this is not a problem as long as we use invariant tools which are not sensitive to the signs of each multipole vector.

Starting with the ℓ multipole vectors one can also construct $\ell(\ell-1)/2 \equiv \lambda$ normal vectors—or normal planes—defined as:

$$\vec{w}^{\,\ell,q} \equiv \hat{n}^{\ell,p} \wedge \hat{n}^{\ell,p'}, \qquad (p \neq p', q = 1 \ldots \lambda). \quad (2)$$

By construction, because the multipole vectors define only directions, the normal vectors also possess reflection symmetry, $\vec{w}^{(\ell,q)} \leftrightarrow -\vec{w}^{(\ell,q)}$. But the normal vectors need not be (and generally are not) of norm unity, so instead of living in $S^2/\mathbb{Z}_2$ the normal vectors belong to the space $\mathbb{R}^3/\mathbb{Z}_2$—which is isomorphic to SO(3), see [57]. We can still break the degeneracies imposed by reflection symmetry by defining all normal vectors so they lie in the same hemisphere as the normal vectors. However, just as before, we should be aware that in doing so we are choosing one of many possible representations for the normal vectors.

To summarize, for $\ell = 2$ there are 2 multipole vectors, $\hat{n}^{(2,1)}$ and $\hat{n}^{(2,2)}$, and only one normal vector, $\vec{w}^{(2,1)} = \hat{n}^{(2,1)} \times \hat{n}^{(2,2)}$; for $\ell = 3$ there are 3 multipole vectors and 3 normal vectors; and so forth. These constitute the basis for the statistical tests defined below.

A. Properties of the tests under reflection symmetry

We will define below, in Sec. II C, a series of tests which are manifestly invariant under the reflection symmetry $\hat{n} \leftrightarrow -\hat{n}$ which characterizes $\mathbb{R}P^2$ (where the multipole vectors live) as well as $\mathbb{R}^3/\mathbb{Z}_2$ (where the associated normal vectors live.)

Our motivation for this remark is that if a given test is not invariant then its validity and usefulness is questionable. In particular, one should be careful not to employ tests which depend on the choice of hemisphere to represent the vectors. This seems to be the case of some of the tests that have been used to estimate the ''planarity'' of the CMB maps, if these tests make use, in one way or another, of the notion of ''average vectors''. The reason there is no such thing as an ''average multipole vector'' or an ''average normal vector'' is simple: the ''vector sum'' operation does not yield a singly valued result due to the reflection symmetry. In fact, the result of ''summing'' two vectors of $\mathbb{R}^3/\mathbb{Z}_2$ would be a degenerated pair of directions:

$$(\pm\vec{v}_1) \oplus (\pm\vec{v}_2) = \begin{cases} \pm\vec{v}_1 \pm \vec{v}_2 \\ \pm\vec{v}_1 \mp \vec{v}_2 \end{cases} . \tag{3}$$

In general, by summing k vectors of $\mathbb{R}^3/\mathbb{Z}_2$ one obtains 2^{k-1} vectors, corresponding to the 2^k possible permutations of the $\pm$ signs of each vector, divided by two to account for the symmetry $\vec{v} \leftrightarrow -\vec{v}$ of the resulting vector. This means, in particular, that the ''average multipole vector'' is in fact an object $2^{\ell-1}$-times degenerated, and that the ''average normal vector'' is an object $2^{\ell(\ell-1)/2-1}$-times degenerated.

Obviously, by fixing a hemisphere to represent all vectors one breaks this degeneracy, but this just hides the plain fact that by doing so one is simply choosing (rather arbitrarily) one of many possible representations, and one of many possible answers for the sums of those vectors. Consequently, unless these degeneracies are properly taken into account (by, e.g., symmetrizing over all possibilities or ordering the results by norm), any test which is derived from the notion of summing multipole or normal vectors is flawed.

B. Global estimates of non-Gaussianity

We will investigate large-scale correlations in the CMB maps within single multipoles and between different multipoles by measuring the alignments between either the multipole vector themselves, or between their associated normal planes. To be sure, there is no upper limit to the number of tests we can devise to search for non-Gaussianities, and in testing any fixed sample such as the CMB one should bear in mind that there are always some statistical tools which will yield a positive detection given some arbitrary criteria.

In practical terms this means that if we perform a large number $\mathcal{N}$ of independent tests on a fixed sample, then we should treat the results of these tests themselves as random numbers. Therefore, when performing many tests on a map and searching for clues of non-Gaussianity one must always look at the complete set of results for those tests and at the total probability (or some global statistic) that the map is a realization of a Gaussian random process. If this global statistic turns out to be very small compared to the typical values for Gaussian maps, then one can look for the particular test (or tests) that is likely responsible for that anomaly. If, however, a certain test turns out to be ''suspicious'' but the global statistic is not anomalously small, then we cannot rule out the possibility that the result for that particular test was just a fluke.

Assuming that random processes are indeed behind the mechanism that generated the sample, we can define a global anomaly statistic in the following sense. Suppose we have $\mathcal{N}$ statistical tests such that each test T_i ($i = 1 \ldots \mathcal{N}$) is a random number in the interval $0 \leq T_i \leq 1$, with normalized probability distribution functions $P_i(T_i)$. Given a sample (a map M) with $T_i = T_i^M$, the probability that a random sample has a value of T_i *higher* than T_i^M is

$$P_{i+}(T_i^M) = \int_{T_i^M}^1 dT P_i(T), \tag{4}$$

and the probability that a random sample has a value of T_i *lower* than T_i^M is

$$P_{i-}(T_i^M) = \int_0^{T_i^M} dT P_i(T) = 1 - P_{i+}(T_i^M). \tag{5}$$

Evidently, for the median value $\bar{T}_i$ we have $P_{i+}(\bar{T}_i) = P_{i-}(\bar{T}_i) = 1/2$. We will *define* the global median statistic of the map M, given the $\mathcal{N}$ tests, to be

$$\begin{aligned} L_{\mathcal{N}}(M) &= \prod_{i=1}^{\mathcal{N}} 2P_{i+}(T_i^M) \times 2P_{i-}(T_i^M) \\ &= 4^{\mathcal{N}} \prod_{i=1}^{\mathcal{N}} P_{i+}(T_i^M)[1 - P_{i+}(T_i^M)], \end{aligned} \tag{6}$$

where the factors of 2 have been inserted for normalization purposes, in order to make $L_{\mathcal{N}}(\bar{M}) = 1$ for a map $\bar{M}$ whose tests are all exactly equal to their median values.

This global anomaly statistic estimates the total probability that the map M does not have too low *and* too high values of the tests T_i. Evidently, any deviation of the tests from the medians will decrease $L_{\mathcal{N}}$. So, the global anomaly statistic is an *unbiased* estimator of the degree of anomalies of a given map, in the sense that both too high and too low correlations would be considered anomalous.

Of course, Eq. (6) is itself an arbitrary definition, and we might as well have used the expectation values instead of the medians to define the global statistic. Indeed, one could switch the roles of the medians with the expectation values in the procedure above and still our results would be very similar. Ideally, we would have computed the Likelihood function, but it turns out that for the numerical strategy we

pursued in this particular work, it would have been impractical to do so.

It should be stressed that the global statistic defined in the sense above should *not* be interpreted as the probability that a particular map was generated by a Gaussian mechanism—it is merely an estimator of how much that particular map deviates from a typical one, given the $\mathcal{N}$ statistical tests of non-Gaussianity. In Sec. II D we construct such tests, and compute their distributions assuming random phases.

C. Statistical tests of isotropy

We now define the statistical tests which will be employed in our analysis of CMB data. We have ensured that all tests are invariant under reflection symmetry, so it makes no difference which hemisphere one chooses to represent the multipole and normal vectors.

The tests have been normalized so that they always fall in the interval $0 \leq T_i \leq 1$. We have generated 3×105 simulated (mock) maps by taking Gaussianly distributed random spherical harmonic components. The resulting PDF's for the tests, assuming Gaussianity, are shown in Figs. 1–4.

1. *S statistic*

The S statistic is a widely used tool [9,11,14,27], and it measures the alignment between normal planes of different multipoles. It is defined as

$$S_{\ell\ell'} \equiv \frac{1}{\lambda\lambda'} \sum_{q=1}^{\lambda} \sum_{q'=1}^{\lambda'} |\vec{w}^{(\ell,q)} \cdot \vec{w}^{(\ell',q')}|, \qquad \ell \neq \ell', \qquad (7)$$

where, as defined above, $\lambda = \ell(\ell-1)/2$. We can also use S in just one multipole, in which case the normalization is a

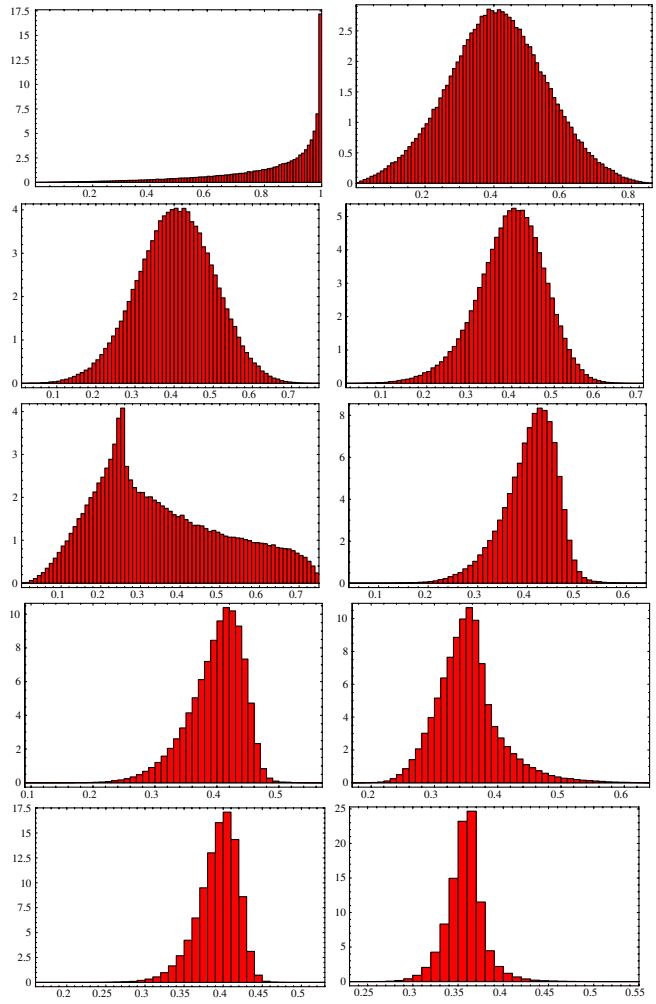

FIG. 1 (color online). Normalized PDF's for the S statistic found by simulating 3×10^5 mock maps, binned in intervals of 0.01. From left to right, top to bottom: S_{22}, S_{23}, S_{24}, S_{25}, S_{33}, S_{34}, S_{35}, S_{44}, S_{45} and S_{55}. In all panels, the horizontal axis correspond to the value of each individual test, and the vertical axis to its normalized PDF.

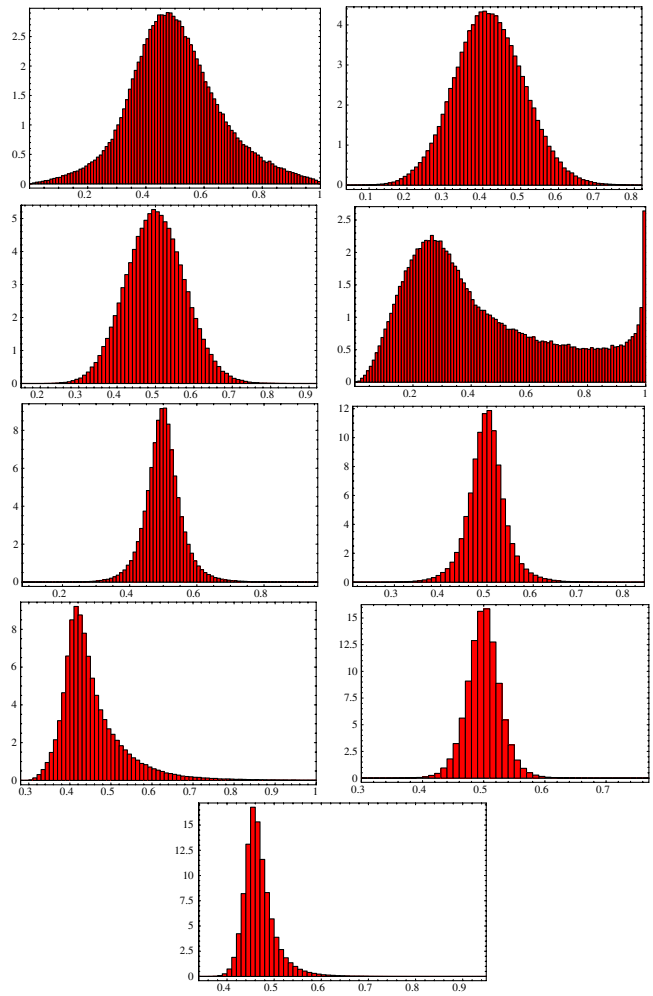

FIG. 2 (color online). Normalized PDF's for the D statistic. From left to right, top to bottom: D_{23}, D_{24}, D_{25}, D_{33}, D_{34}, D_{35}, D_{44}, D_{45} and D_{55}.

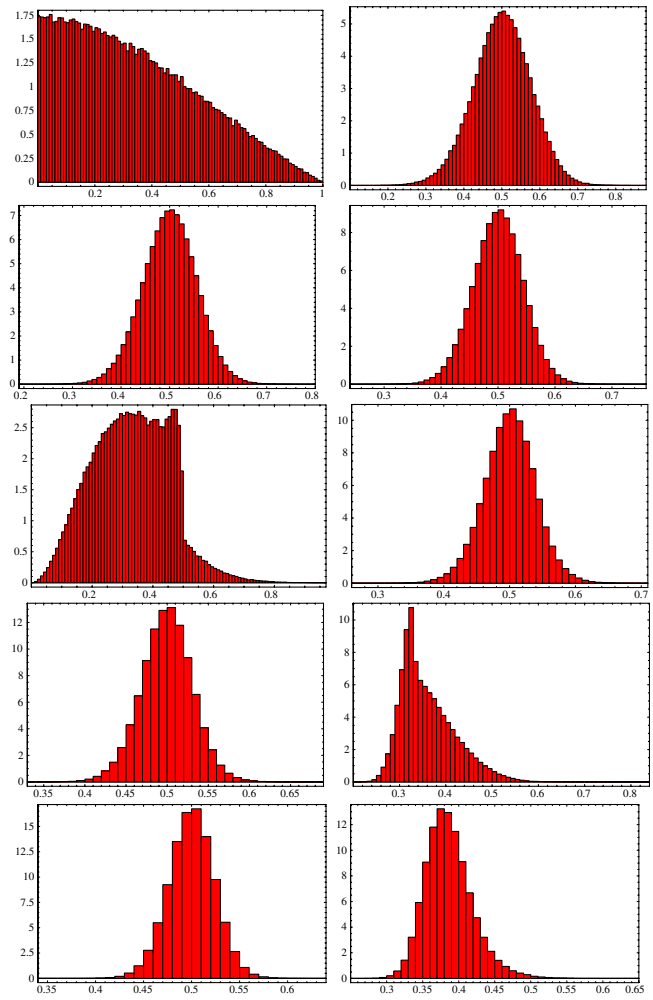

FIG. 3 (color online). Normalized PDF's for the R statistic. From left to right, top to bottom: R_{22}, R_{23}, R_{24}, R_{25}, R_{33}, R_{34}, R_{35}, R_{44}, R_{45} and R_{55}.

bit different:

$$S_{\ell\ell} \equiv \frac{2}{\lambda(\lambda-1)} \sum_{q,q'>q}^{\lambda} |\vec{w}^{(\ell,q)} \cdot \vec{w}^{(\ell,q')}|. \qquad (8)$$

The statistic $S_{\ell\ell}$ measures the "self-alignment" of the normal vectors, and is related to the planarity tests [5,14].

2. D statistic

This is analogous to the S statistic, but the D test disregards the norm of the normal vectors [9,11,14,27]:

$$D_{\ell\ell'} \equiv \frac{1}{\lambda\lambda'} \sum_{q=1}^{\lambda} \sum_{q'=1}^{\lambda'} |\hat{w}^{(\ell,q)} \cdot \hat{w}^{(\ell',q')}|, \qquad \ell \neq \ell'. \qquad (9)$$

We can also use the D statistic within a single multipole, as was done for S. However, this test only gives nontrivial information for $\ell \geq 3$. With the proper normalization we have

$$D_{\ell\ell} \equiv \frac{2}{\lambda(\lambda-1)} \sum_{q,q'>q}^{\lambda} |\hat{w}^{(\ell,q)} \cdot \hat{w}^{(\ell,q')}|, \qquad \ell \geq 3. \quad (10)$$

3. R statistic

A similar tool is the R statistic, which measures alignments in essentially the same way as the S statistic, but it uses the multipole vectors instead of the normal vectors:

$$R_{\ell\ell'} \equiv \frac{1}{\ell\ell'} \sum_{p=1}^{\ell} \sum_{p'=1}^{\ell'} |\hat{n}^{(\ell,p)} \cdot \hat{n}^{(\ell',p')}|, \qquad \ell \neq \ell'. \qquad (11)$$

Within a single multipole, the R statistic is suitably defined as

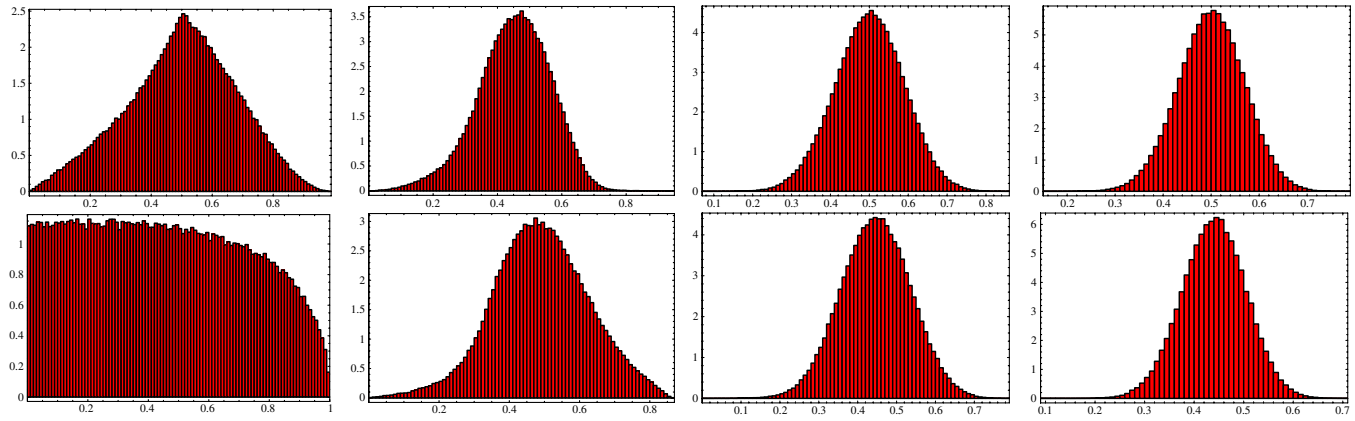

FIG. 4 (color online). Normalized PDF's for the N and W statistics—alignments of the multipole (N) and normal (W) vectors with a particular direction in the sky. Top line, from left to right: N_2, N_3, N_4, N_5. Bottom line, from left to right: W_2, W_3, W_4, W_5.

$$R_{\ell\ell} \equiv \frac{2}{\ell(\ell-1)} \sum_{p,p'>p}^{\ell} |\hat{n}^{(\ell,p)} \cdot \hat{n}^{(\ell,p')}|. \qquad (12)$$

4. B statistic

We can also test if the multipole vectors align with the normal vectors. Hence we define the B statistic:

$$B_{\ell\ell'} \equiv \frac{1}{\lambda\ell'} \sum_{q=1}^{\lambda} \sum_{p'=1}^{\ell'} |\vec{w}^{(\ell,q)} \cdot \hat{n}^{(\ell',p')}|, \qquad \ell \neq \ell'. \qquad (13)$$

Within a single multipole, the B statistic only gives non-trivial information for $\ell \geq 3$, and we have

$$B_{\ell\ell} \equiv \frac{1}{\lambda(\ell-2)} \sum_{q}^{\lambda} \sum_{p}^{\ell} |\vec{w}^{(\ell,q)} \cdot \hat{n}^{(\ell,p)}|, \qquad \ell \geq 3. \qquad (14)$$

Notice that, as opposed to the S, D and R statistics, the B statistic for $\ell \neq \ell'$ is not symmetric, $B_{\ell\ell'} \neq B_{\ell'\ell}$. For simplicity, in the present approach we have only considered the cases $B_{\ell\ell'}$ where $\ell \leq \ell'$.

5. N statistic

We can test if the multipole vectors align in a particular direction $\hat{Z}$ by using the N statistic:

$$N_\ell \equiv \frac{1}{\ell} \sum_{p=1}^{\ell} |\hat{n}^{(\ell,p)} \cdot \hat{Z}|. \qquad (15)$$

6. W statistic

We can also test if the normal vectors align in a particular direction $\hat{Z}$ by using the W statistic:

$$W_\ell \equiv \frac{1}{\lambda} \sum_{q=1}^{\ell} |\vec{w}^{(\ell,q)} \cdot \hat{Z}|. \qquad (16)$$

Note that the test $S^{(4,4)}$ of Ref. [14] is a combination of W_2 and W_3, namely, $S^{(4,4)} = (W_2 + 3W_3)/4$.

D. Likelihoods

With the tests defined above we can now compute global statistic as in Eq. (6). However, we have decided not to include the alignment tests N and W in the analysis, as they test correlations with an *a priori* direction, which we find rather arbitrary compared to the other tests. Nevertheless, it should be noted that there are significant correlations between the quadrupole and the octopole with both the ecliptic plane and the direction of the cosmic dipole. Although these correlations appear to be too strong or too weak only at >95% C.L. as measured by our tests N_ℓ and W_λ, when combined in the statistic $S^{(4,4)}$ of Copi *et al.* [27], we obtain a result which is >99.5% C.L. These correlations have been treated in much greater detail in Refs. [9,14,21,27].

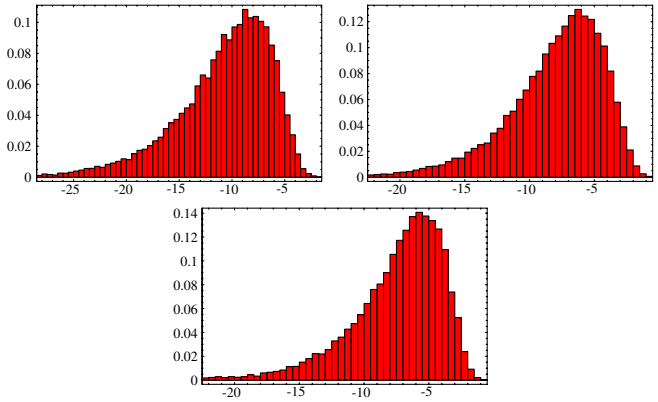

FIG. 5 (color online). Normalized histograms of $\log_{10}L_{38}(S, D, R, B)$ (left panel), $\log_{10}L_{29}(S, D, R)$ (center) and $\log_{10}L_{29}(S, R, B)$ (right), obtained by simulating 25 000 mock maps.

Using the 38 tests S, D, R and B above, we can define a global anomaly statistic, $L_{38}(S, D, R, B)$, as in Eq. (6). We have computed L_{38} for 25 000 random maps, and we show a normalized histogram for $\log_{10}L_{38}$ in Fig. 5 (left panel.)

Since we have 38 tests but only 28 independent random degrees of freedom in the $\ell = 2 - 5$ multipoles, we have found useful to define global anomaly statistic using a subset of the complete set of tests. We have thus defined the statistic $L_{29}(S, D, R)$ using the tests S, D and R, and $L_{29}(S, R, B)$, using the S, R and B tests. Their normalized histograms are also shown in Fig. 5 (center and right panels.)

III. CMB MAPS

In this work, we use five WMAP CMB maps (three derived from the 1-year data [1] and two derived from the 3-year data [58]): the 1-year and 3-year co-added maps [59]; the 1-year and 3-year ILC maps [3,58]; and the TOH map [15].

The co-added WMAP map results from the combination of the eight differential assemblies (DA) [59] in the Q-, V-, and W-bands, listed above, using the following inverse-variance noise weights method. Thus, for any co-added map, the temperature of pixel n is given by

$$T(n) = \frac{\sum_{i=1}^{8} T_i(n)/\sigma_i^2(n)}{\sum_{i=1}^{8} 1/\sigma_i^2(n)}, \qquad (17)$$

where $T_i(n)$ is the sky map for the DA i with the foreground galactic signal subtracted, and where

$$\sigma_i^2(n) \equiv \sigma_{0,i}^2/N_{\rm obsi}(n) \qquad (18)$$

is the pixel-noise *per* observation for DA i. The eight values of $\sigma_{0,i}^2$ are the pixel-noise for DA i, and can be found for each set of released maps in [60].

The WMAP 1-year Internal Linear Combination map (ILC-1 yr) [3] has been built mostly to convey a visual information of CMB anisotropies. It is composed by the five WMAP temperature intensity maps, through a weighted linear combination, to minimize Galactic foreground contamination in 12 regions of the sky, eleven of which lie within the Galactic plane and one which lies outside it. The ILC-1 yr map is not reliable for quantitative CMB analysis, but in this work we use it only for the completeness of our analysis. The 3-year WMAP ILC map (ILC-3 yr) [58], however, brings some improvements over the ILC-1 yr, mainly by dealing with the regions selected for Galactic foreground estimates, which make it a reliable estimator of the CMB signal for large angular scales ($> 10°$) and, therefore, suitable for our analysis since we are interested in $\ell = 2 - 5$.

The 1- and 3-yr ILC maps are described, respectively, in [3,58], but it is worth mentioning here the differences between them. The 1-yr and 3-yr ILC maps are both weighted combinations of the maps, band-averaged within each of the five WMAP frequency bands. They corrected the bias due to the foreground removal method by dividing the sky into 12 regions, minimizing the variance of the linear combination of the 5 frequencies for each region and then weighting the final combined map according to the region. There was an additional bias correction, in the 3-yr ILC map, that was done after using 100 Monte Carlo simulations with a variable spectrum Galaxy model as input [58]. The WMAP team claims the residual error in the 3-year ILC map is less than 5 μK in angular scales greater than 10°, being a reliable estimate of the CMB signal, with negligible instrument noise, over the full sky.

The TOH map [15] was constructed with no assumption about the CMB power spectrum, foregrounds or noise properties. The only consideration was the Planckian nature of the CMB temperature spectrum. This map is formed by the combination of the five WMAP bands considering weights that depend both on angular scale and distance to the Galactic plane. The cleaning process is done in multipole space a_{lm}, weighted also by the beam function of each channel (W-band has four channels, Q- and V-band have two channels each, and K- and Ka-band have one channel each). They obtain weighting coefficients similar to those used by the WMAP team on large scales.

IV. STATISTICS OF LARGE-ANGLE ANISOTROPIES

Given a CMB map, the harmonic components $a_{\ell m}$ can be extracted using HEALPix [55], and the multipole vectors and their statistics can be easily computed. In this analysis we will use the five maps described above, plus the TOH map cleaned with the mask "M6" given in [13,15]. For all maps we have used the Kp2 mask based on 3-year WMAP data [3,4], then we remove their residual monopole and dipole components. It should also be noted that the relativistic Doppler correction to the quadrupole is an important factor that must be subtracted from the maps, since it corresponds to a nonprimary source of the quadrupole [14,27].

In Table I we present an abridged version of the tests that were defined in Sec. II C. For an easier interpretation of the results, we show the probabilities $P_+(T_i)$ that a random map would have *higher* values for the test T_i than the value for that test in the actual CMB maps. So, for instance, for the test S_{22} and for the co-added 1-yr map we quote the value $P_+(S_{22}) = 0.294$. This means that the probability that a random map has a value of S_{22} which is higher than the value obtained for the map co-added 1-yr is 29.4%. Therefore, in Table I, any values which are too close to either zero or one should be viewed with suspicion.

It can be immediately seen from Table I that the quadrupole-octopole alignment (revealed by S_{23}, D_{23} and B_{23}) is robust in all maps, as has been noted by [5,9,13,14,20,21,27]. Our results confirm that the probability that a random map has higher quadrupole-octopole alignment, as measured by S_{23}, is approximately 1–2%.

Table I also reveals (through the self-alignments S_{33}, D_{33}, R_{33} and B_{33}) that, at least for our set of invariant tests, there is no evidence that the octopole is significantly "planar," in the sense defined by these tests.

There are other anomalies for $\ell \geq 3$ as well: we find that the octopole and hexadecupole ($\ell = 4$) are misaligned to a very significant degree, with a probability in the range 1%–4% for the test S_{34} and 5%–20% for the tests D_{34} and R_{34}. The triandabipole ($\ell = 5$) also seems substantially misaligned with the octopole $\ell = 3$, with a probability in the range 4%–8% for the test S_{35}. These results, plus the fact that the octopole is significantly aligned with the dipole axis, give further support to the conjecture known as the "axis of evil" [21].

Another apparent anomaly that is revealed by Table I is the self-alignment of the multipoles $\ell = 4$ and $\ell = 5$, indicated by the values of P_+ for S_{44}, D_{55}, R_{44} and R_{55}.

Not shown in Table I are the results for the tests N and W, using as *a priori* directions to be tested against the dipole axis, the ecliptic plane and the galactic plane. The results for these 24 tests indicate that there are significant alignments of the quadrupole and octopole with the direction defined by the cosmic dipole [5,9,13,14,20,21,27]: $W_2^{\text{Dipole}} \sim 0.10 - 0.01$ and $W_3^{\text{Dipole}} \sim 0.03$–$0.05$ depending on the choice of map. We also confirm the results of Copi *et al.* [9,14,20,27], who found strong correlations of the quadrupole and octopole with the ecliptic plane: we get $W_2^{\text{Ecliptic}} \sim 0.83$–$0.98$ and $W_3^{\text{Dipole}} \sim 0.93$–$0.98$ depending on the choice of map. If combined into a single test, the tests W_2 and W_3 give rise to very significant correlations, both with the cosmic dipole and with the ecliptic plane. For all other multipoles and directions we have found no significant alignments using our tests.

TABLE I. Probabilities P_+ for the tests S, D, R and B. These are the probabilites that a random map would have values for the tests S, D, R and B which are *higher* than the map's values. The probability that a random map has a value *lower* than the map's is simply $P_- = 1 - P_+$.

Statistic	Co-added 1-yr	Co-added 3-yr	ILC 1-yr	ILC 3-yr	$\mathrm{TOH}_{\mathrm{Mask6}}$	$\mathrm{TOH}_{\mathrm{Kp2}}$
S_{22}	0.294	0.242	0.242	0.437	0.437	0.294
S_{23}	0.011	0.011	0.007	0.021	0.006	0.017
S_{24}	0.519	0.637	0.519	0.803	0.774	0.519
S_{25}	0.922	0.903	0.937	0.903	0.864	0.913
S_{33}	0.457	0.530	0.457	0.549	0.270	0.586
S_{34}	0.965	0.973	0.978	0.978	0.990	0.965
S_{35}	0.957	0.943	0.957	0.921	0.921	0.921
S_{44}	0.960	0.960	0.975	0.985	0.905	0.960
S_{45}	0.750	0.750	0.750	0.750	0.750	0.750
S_{55}	0.714	0.714	0.714	0.714	0.664	0.689
D_{23}	0.034	0.046	0.031	0.056	0.019	0.051
D_{24}	0.771	0.884	0.771	0.922	0.937	0.085
D_{25}	0.854	0.786	0.907	0.744	0.550	0.786
D_{33}	0.268	0.333	0.276	0.351	0.187	0.361
D_{34}	0.802	0.888	0.916	0.916	0.965	0.850
D_{35}	0.711	0.711	0.797	0.607	0.375	0.607
D_{44}	0.913	0.913	0.913	0.913	0.623	0.913
D_{45}	0.342	0.342	0.342	0.342	0.786	0.499
D_{55}	0.970	0.970	0.989	0.970	0.970	0.970
R_{22}	0.828	0.931	0.880	0.647	0.647	0.811
R_{23}	0.071	0.030	0.091	0.091	0.176	0.115
R_{24}	0.576	0.767	0.710	0.896	0.817	0.576
R_{25}	0.823	0.759	0.914	0.759	0.598	0.759
R_{33}	0.424	0.506	0.424	0.533	0.294	0.533
R_{34}	0.706	0.902	0.937	0.937	0.986	0.902
R_{35}	0.834	0.834	0.899	0.834	0.834	0.834
R_{44}	0.892	0.939	0.968	0.968	0.485	0.939
R_{45}	0.338	0.198	0.198	0.198	0.670	0.338
R_{55}	0.977	0.977	0.977	0.977	0.945	0.945
B_{23}	0.940	0.920	0.920	0.920	0.968	0.883
B_{24}	0.139	0.192	0.065	0.192	0.033	0.117
B_{25}	0.344	0.256	0.392	0.256	0.806	0.298
B_{33}	0.696	0.582	0.644	0.540	0.749	0.554
B_{34}	0.651	0.426	0.344	0.262	0.189	0.506
B_{35}	0.591	0.414	0.506	0.414	0.784	0.414
B_{44}	0.079	0.116	0.201	0.249	0.300	0.116
B_{45}	0.336	0.336	0.497	0.497	0.497	0.336
B_{55}	0.444	0.444	0.338	0.338	0.136	0.233

TABLE II. Total likelihoods $L_{38}(S, D, R, B)$, $L_{38}(S, D, R)$ and $L_{29}(S, R, B)$. The normalized histograms for the global anomaly statistics found by simulating 25 000 maps are shown in Fig. 5.

Global Statistics	Co-added 1-yr	Co-added 3-yr	ILC 1-yr	ILC 3-yr	$\mathrm{TOH}_{\mathrm{Mask6}}$	$\mathrm{TOH}_{\mathrm{Kp2}}$
$L_{38}(S, D, R, B)$	3.2×10^{-13}	2.0×10^{-14}	7.7×10^{-18}	3.6×10^{-14}	3.7×10^{-16}	4.8×10^{-12}
$L_{29}(S, D, R)$	1.7×10^{-11}	4.3×10^{-13}	5.2×10^{-15}	5.1×10^{-13}	3.0×10^{-13}	1.3×10^{-10}
$L_{29}(S, R, B)$	5.1×10^{-10}	4.3×10^{-11}	3.0×10^{-12}	8.8×10^{-11}	3.9×10^{-12}	3.6×10^{-9}

We can estimate the global statistics for the CMB maps of Table I. This is shown in Table II for the statistics $L_{38}(S, D, R, B)$, $L_{29}(S, D, R)$ and $L_{29}(S, R, B)$. Comparing the values of Table II with the normalized histograms of Fig. 5, we can see that, apart from the TOH map with the Kp2 mask applied, which lies within the $\sim$30% of random maps with lowest global anomaly statistics, all remaining maps fall within the $\sim$10% of random maps with lowest global anomaly statistics. The global statistics are particularly small for the 1-year ILC map, which, as discussed, is probably contaminated by residual foregrounds.

V. CONCLUSIONS

We have applied 38 tests of non-Gaussianity, as well as 8 tests of alignments with 3 distinct preferred directions, on the most widely used CMB maps based on 1-year and 3-year WMAP data. In order to properly analyze the set of tests performed in the WMAP maps, we have introduced the notion of a global anomaly statistic to estimate the relevance of the low-multipoles tests of non-Gaussianity for each map. A cautionary note is sounded by the global anomaly statistic: this criterium shows that the CMB maps we studied have rather low statistics, but they still lie within the $\sim$10% of random maps with lowest global anomaly statistics, meaning that 90% of the Gaussian mock maps have higher global anomaly statistics than the CMB maps.

We confirm the well-known alignment between the quadrupole and the octopole, and we found other significant levels of alignment between the octopole and the hexadecupole. Moreover, we detected that the hexadecupole and the $\ell = 5$ multipole have significantly low levels of self-alignments (see Table I). Taken individually, these tests show non-Gaussian features at more than 95% C.L. On the other hand, no significant evidence of self-alignment (which is related to the planarity) was found for the octopole.

Regarding correlations with the directions of the cosmic dipole, the ecliptic plane or the galactic plane, we have confirmed the correlations of the quadrupole and octopole with the cosmic dipole, as well as the correlation of the octopole with the ecliptic plane. For all other multipoles and directions we have found no significant alignments.

In conclusion, we have found intriguing evidence of nonrandom alignments in the multipoles $\ell = 2 - 5$, which have not only survived, but have indeed been strengthened by the recently released 3-year WMAP data.

ACKNOWLEDGMENTS

L. R. A. would like to thank João Barata and for useful remarks on the properties of projective spaces, and Dominik Schwarz for useful comments on the Doppler Quadrupole. We have benefitted from the use of the HEALPix package [55]. We also acknowledge the use of the Legacy Archive for Microwave Background Data Analysis (LAMBDA, [60]), which is supported by the NASA Office of Space Science. L. R. A. received support from CNPq, Grant No. 475376/2004-8. A. B. is supported by MCT PCI/DTI/7B. I. S. F. is supported by CAPES. T. V. and C. A. W. acknowledge support from CNPq Grants Nos. 305219/2004-9-FA and 307433/2004-8-FA, respectively.

[1] C. L. Bennett *et al.*, Astrophys. J. Suppl. Ser. **148**, 1 (2003).
[2] D. Spergel *et al.*, Astrophys. J. Suppl. Ser. **148**, 175 (2003).
[3] C. L. Bennett *et al.*, Astrophys. J. Suppl. Ser. **148**, 97 (2003).
[4] D. Spergel *et al.*, astro-ph/0603449.
[5] A. de Oliveira-Costa *et al.*, Phys. Rev. D **69**, 063516 (2004).
[6] G. Efstathiou, Mon. Not. R. Astron. Soc. **348**, 885 (2004).
[7] E. Gaztañaga *et al.*, Mon. Not. R. Astron. Soc. **346**, 47 (2003).
[8] S. Prunet, J.-P. Uzan, F. Bernardeau, and T. Brunier, Phys. Rev. D **71**, 083508 (2005).
[9] C. J. Copi, D. Huterer, and G. D. Starkman, Phys. Rev. D **70**, 043515 (2004).
[10] H. K. Eriksen *et al.*, Astrophys. J. **612**, 633 (2004).
[11] G. Katz and J. Weeks, Phys. Rev. D **70**, 063527 (2004).
[12] J. Weeks, astro-ph/0412231.
[13] A. de Oliveira-Costa and M. Tegmark, Phys. Rev. D **74**, 023005 (2006).
[14] D. J. Schwarz *et al.*, Phys. Rev. Lett. **93**, 221301 (2004).
[15] M. Tegmark, A. de Oliveira-Costa, and A. Hamilton, Phys. Rev. D **68**, 123523 (2003).
[16] K. Górski *et al.*, Astrophys. J. **464**, L11 (1996).
[17] E. Wright *et al.*, Astrophys. J. **464**, L21 (1996).
[18] E. Gaztañaga *et al.*, Mon. Not. R. Astron. Soc. **346**, 47 (2003).
[19] A. Slosar, U. Seljak, and A. Makarov, Phys. Rev. D **69**, 123003 (2004).
[20] C. Copi, D. Huterer, D. Schwarz, and G. Starkman, astro-ph/0605135.
[21] K. Land and J. Magueijo, Phys. Rev. Lett. **95**, 071301 (2005).
[22] P. Bielewicz, K. M. Górski, and A. J. Banday, Mon. Not. R. Astron. Soc. **355**, 1283 (2004).
[23] P. Bielewicz *et al.*, Astrophys. J. **635**, 750 (2005).
[24] F. K. Hansen, A. J. Banday, and K. M. Górski, Mon. Not. R. Astron. Soc. **354**, 641 (2004).

[25] H. K. Eriksen *et al.*, Astrophys. J. **605**, 14 (2004); **609**, 1198(E) (2004).
[26] A. Bernui *et al.*, astro-ph/0601593.
[27] C. J. Copi *et al.*, Mon. Not. R. Astron. Soc. **367**, 79 (2006).
[28] K. Land and J. Magueijo, Mon. Not. R. Astron. Soc. **357**, 994 (2005).
[29] A. Bernui, B. Mota, M. J. Rebouças, and R. Tavakol, astro-ph/0511666.
[30] Y. Wiaux, P. Vielva, E. Martinez-Gonzalez, and P. Vandergheynst, Phys. Rev. Lett. **96**, 151303 (2006).
[31] P. Vielva *et al.*, Astrophys. J. **609**, 22 (2004).
[32] M. Cruz *et al.*, Mon. Not. R. Astron. Soc. **356**, 29 (2005).
[33] M. Cruz *et al.*, astro-ph/0603859.
[34] F. K. Hansen *et al.*, Astrophys. J. **607**, L67 (2004).
[35] J. McEwen, M. Hobson, A. Lasenby, and D. Mortlock, astro-ph/0604305.
[36] A. Bernui, C. Tsallis, and T. Villela, Phys. Lett. A **356**, 426 (2006).
[37] J.-P. Luminet *et al.*, Nature (London) **425**, 593 (2003).
[38] B. Mota *et al.*, Classical Quantum Gravity **21**, 3361 (2004).
[39] C. Contaldi *et al.*, J. Cosmol. Astropart. Phys. 07 (2003) 002.
[40] J. Cline, P. Crotty, and J. Lesgourgues, J. Cosmol. Astropart. Phys. 09 (2003) 010.
[41] B. Feng and X. Zhang, Phys. Lett. B **570**, 145 (2003).
[42] S. Tsujikawa, R. Maartens, and R. Brandenberger, Phys. Lett. B **574**, 141 (2003).
[43] Y.-S. Piao, B. Feng, and X. Zhang, Phys. Rev. D **69**, 103520 (2004).
[44] M. Kawasaki and F. Takahashi, Phys. Lett. B **570**, 151 (2003).
[45] J. Martin and C. Ringeval, Phys. Rev. D **69**, 083515 (2004).
[46] J. Martin and C. Ringeval, Phys. Rev. D **69**, 127303 (2004).
[47] J. Martin and C. Ringeval, J. Cosmol. Astropart. Phys. 01 (2005) 007.
[48] T. Jaffe *et al.*, Astrophys. J. **629**, L1 (2005).
[49] L. Cayón *et al.*, Mon. Not. R. Astron. Soc. **369**, 598 (2006).
[50] T. Gosh, A. Hajian, and T. Souradeep, astro-ph/0604279.
[51] L. R. Abramo and L. Sodré, Jr., astro-ph/0312124.
[52] L. R. Abramo, L. Sodré, Jr., and C. A. Wuensche, astro-ph/0605269.
[53] K. T. Inoue and J. Silk, astro-ph/0602478.
[54] A. Rakic, S. Rasanen, and D. J. Schwarz, Mon. Not. R. Astron. Soc. **369**, L27 (2006).
[55] K. M. Górski *et al.*, Astrophys. J. **622**, 759 (2005).
[56] R. C. Helling, P. Schupp, and T. Tesileanu, astro-ph/0603594.
[57] M. Nakahara, *Geometry, Topology and Physics* (Institute of Physics Publishing, Bristol and Philadelphia, 1990).
[58] G. Hinshaw *et al.*, astro-ph/0603451.
[59] G. Hinshaw *et al.*, Astrophys. J. Suppl. Ser. **148**, 135 (2003).
[60] http://lambda.gsfc.nasa.gov/product/map/current/.